

The Power Spectrum of Flux Limited X-Ray Galaxy Cluster Surveys

Ariel Zandivarez^{1,2}, Mario. G. Abadi^{2,3} and Diego G. Lambas^{2,3}

¹ *Facultad de Matemática Astronomía y Física, Universidad Nacional de Córdoba, Argentina*

² *Grupo de Investigaciones en Astronomía Teórica y Experimental, IATE, Observatorio Astronómico, Laprida 854, Córdoba, Argentina*

³ *Consejo de Investigaciones Científicas y Técnicas de la República Argentina*

27 October 2018

ABSTRACT

We compute the redshift space power spectrum of two X-ray cluster samples: the X-ray Brightest Abell Cluster Sample (XBACS) and the Brightest Cluster Sample (BCS) using the method developed by Feldman, Kaiser & Peacock. The power spectrums derived for these samples are in agreement with determinations of other optical and X-ray cluster samples. For XBACS we find the largest power spectrum amplitude expected given the high richness of this sample ($R \geq 2$). In the range $0.05h\text{Mpc}^{-1} < k < 0.4h\text{Mpc}^{-1}$ the power spectrum shows a power law behavior $P(k) \propto k^n$ with an index $n \simeq -1.2$. In a similar range $0.04h\text{Mpc}^{-1} < k < 0.3h\text{Mpc}^{-1}$ BCS power spectrum has a smaller amplitude with index $n \simeq -1.0$. We do not find significant evidence for a peak at $k \simeq 0.05h\text{Mpc}^{-1}$ suggesting that claims such of feature detections in some cluster samples could relay on artificial inhomogeneities of the data. We compare our results with power spectrum predictions derived by Moscardini et al. within current cosmological models (LCDM and OCDM). For XBACS we find that both models underestimate the amplitude of the power spectrum but for BCS there is reasonably good agreement at $k \gtrsim 0.03h\text{Mpc}^{-1}$ for both models.

Key words: galaxies: clusters: general-large scale structure of Universe-X-rays: galaxies

1 INTRODUCTION

The distribution of matter at very large scales can be traced using galaxy clusters that are the largest virialized objects in the Universe. This distribution is deeply connected to the fluctuations in the primordial density field since at very large scales gravitational effects are still linear. Assuming a Gaussian distribution of fluctuations the two point correlation function $\xi(r)$ or the power spectrum $P(k)$ are statistical tools suitable to give a complete description of the matter distribution. From a mathematical point of view any of these functions are equivalent since they form a Fourier transform pair. In the last years, considerably effort has been carried out applying these statistics to different observational samples of galaxy clusters.

The Abell (1958) catalogue and its extension Abell-ACO (Abell, Corwin & Olowin, 1989), constructed by visual inspection of Palomar photographic plates, is probably the most widely used cluster survey. In pioneering works Peacock & West (1992) and Jing & Valdarnini (1993) have computed the power spectrum for different Abell cluster samples. At large wave-numbers $k \gtrsim 0.05h\text{Mpc}^{-1}$ they

found a power law behavior $P(k) \propto k^n$ with an index $-1.4 \lesssim n \lesssim -1.7$. At lower wave-numbers, $k \lesssim 0.05h\text{Mpc}^{-1}$, there is a striking flattening of the power spectrum changing dramatically the value of n . More recently, Einasto et al. (1997) and Retzlaff et al. (1998) using other Abell-ACO samples found a peak at $k \sim 0.04 - 0.05h\text{Mpc}^{-1}$ near the wave-number where the flattening starts. Miller & Batuski (2000) reanalyzing an Abell-ACO sample claim that this peak is only present due to the inclusion of clusters of richness $R = 0$ and clusters with estimated (not measured) redshifts. They also point out that $R = 0$ clusters are outside the statistical sample of Abell (1958) and do not constitute a fair sample. It should be noted the importance of such features due to the deep link with primordial mass power spectrum of current cosmological models.

It has been claimed that projection effects can be strongly present in optical cluster catalogue and could increase artificially their power spectrum amplitude. One attempt to minimize subjectivities present in optically selected cluster catalogue is the identification of clusters in photographic plates by means of automatic computer algorithms like in the APM cluster survey (Dalton et al. 1997). The

power spectrum obtained by Tadros, Efstathiou & Dalton (1998) for this cluster sample shows a smooth transition from positive to negative slopes near $k = 0.03 - 0.04 h \text{Mpc}^{-1}$ without the detection of any peak. Another way to avoid this problem is the identification of clusters in the X-ray band where the highly peaked emission in cluster centers minimizes the probability of projection effects. Bohringer et al. (1998) present the ROSAT ESO Flux Limited X-ray (REFLEX) survey that is an optically confirmed X-ray cluster sample in the southern hemisphere. For a relatively small subsample they also present one of the highest power spectrum amplitude for a cluster sample without detecting the presence of a peak. There are another two X-ray flux limited cluster catalogue constructed from the ROSAT all-sky survey (RASS): the X-ray Brightest Abell-type Cluster sample (XBACS; Ebeling et al. 1996) and the Brightest Cluster Sample (BCS; Ebeling et al. 1998). Recently, an extension of BCS to a lower flux limit has been released forming the extended BCS (EBCS, Ebeling et al. 2000). This sample is constructed from the extended X-ray emission of RASS, while the XBACS is based on previously optically selected clusters. In a recent paper, Moscardini et al. (2000) provide predictions for the correlation function and power spectrum of X-ray flux limited surveys for different cosmological models. They apply their models to XBACS, BCS and REFLEX following the non-linear evolution of clustering and using theoretical and observational relations between intrinsic properties of clusters like mass, luminosity and temperature.

The aim of this paper is to estimate the redshift space power spectrum of XBACS and BCS in order to compare with observational results for different samples and model predictions. The paper is organized in the following way: In section 2 we describe the X-ray cluster samples to be analyzed. In section 3 we present the method applied to estimate the power spectrum of a flux limited sample with the derivation of the corresponding errors. In section 4 the main results are discussed and we present the conclusions in section 5.

2 XBACS AND BCS

In this section we briefly describe the main characteristics of the samples relevant for the power spectrum estimation. The XBACS comprise 242 Abell-ACO X-ray confirmed clusters distributed in the whole celestial sphere excluding the strip of low galactic latitude $|b_{lim}| < 20^\circ$. The flux limit of the sample is $F_{lim} = 5 \times 10^{-12} \text{ erg s}^{-1} \text{ cm}^{-2}$ in the energy range 0.1-2.4 keV and the redshift limit is $z = 0.2$. Ebeling et al. (1996) estimate that the overall completeness of the XBACS is $\gtrsim 80\%$ at the above F_{lim} . This sample is free of volume incompleteness since is constructed from the brightest Abell/ACO clusters which suffer of incompleteness problems only for poorest clusters (Plionis & Kolokotronis 1998).

The original BCS consists of 201 clusters distributed in the northern equatorial hemisphere ($\delta \geq 0^\circ$) with the same cut in galactic latitude $|b_{lim}| < 20^\circ$ and a redshift limit $z \leq 0.3$. The corresponding flux limit is similar to XBACS ($F_{lim} = 4.4 \times 10^{-12} \text{ erg s}^{-1} \text{ cm}^{-2}$) in the same band with a completeness of $\sim 90\%$. The extension of BCS (Ebeling

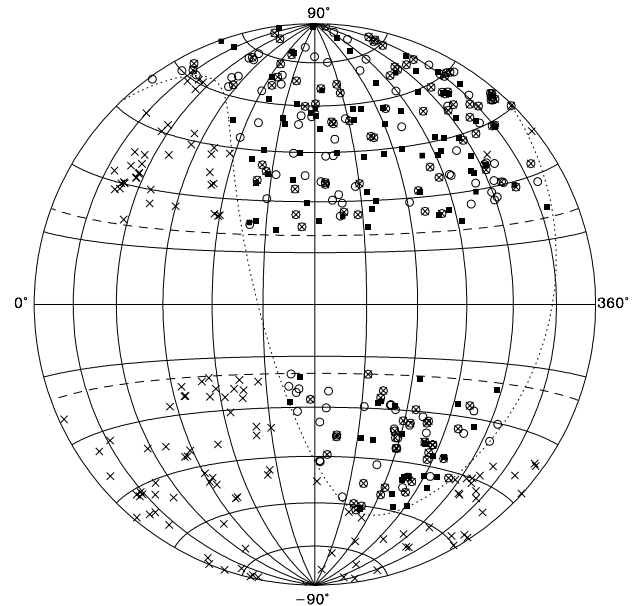


Figure 1. Aitoff projection using galactic coordinate of the distribution of XBACS (crosses) and BCS (original BCS are shown as open circles and its extension to a lower flux limit as filled squares). The dashed lines show the limit $|b_{lim}| \geq 20^\circ$ and the dotted line $\delta = 0^\circ$

et al. 2000) includes 100 additional clusters up to a lower limit $F_{lim} = 2.8 \times 10^{-12} \text{ erg s}^{-1} \text{ cm}^{-2}$. These two samples form jointly the EBCS comprising 301 clusters with a nominal completeness relatively low $\sim 75\%$. Ebeling et al. (1996, 1998 and 2000) give right ascensions, declinations (J2000.0) and redshifts for XBACS, BCS and its extension, respectively.

In Figure 1 we show the angular distribution in galactic coordinates of XBACS (crosses) and BCS (open circles for the original sample and filled squares for its extension). The superposition of open circles and crosses indicate that $\gtrsim 50\%$ of BCS are included in the XBACS.

3 POWER SPECTRUM ESTIMATION

3.1 Introduction

In this section we outline the scheme applied to estimate the redshift space power spectrum. If a redshift survey is used to compute the power spectrum of a distribution, then the resulting power spectrum is the convolution of the real spectrum with the catalogue window function. This window function depends on the geometry of the survey and on the technique employed to calculate it and should be as narrow as possible. Several authors present different methods to estimate the redshift space power spectrum of a sample. In a pioneer work of Feldman, Kaiser & Peacock (1994, hereafter FKP) provide a suitable method for a flux limited sample with a detailed analysis of errors. Tegmark (1995) present another way to calculate the power spectrum that maximizes the spectral resolution for different survey geometries. Tadros & Efstathiou (1996) give a variation of FKP, but for

Table 1. Parameters of the fitting formulae (eq. 2). r_{max} units are $h^{-1}\text{Mpc}$

sample	x	y	N_{max}	r_{max}
XBACS	1.96	2.73	28.12	197.54
BCS	3.13	1.59	16.22	74.83

a volume limited sample. Analyzing different methods to compute the power spectrum, Tegmark et al. (1998) show that FKP method is the most appropriate for wave-numbers greater than the point where the value of the window function decrease a factor 2 of its value at the origin. We apply the method derived by FKP in the version described by Hoyle et al. (1999). This method is suitable for our samples due to its simple quasi-spherical geometry (Sutherland et al. 1999).

3.2 Spatial Distribution

We have used the standard transformation from redshift z to comoving distance r for a model universe with a dimensionless density parameter equal to unity and a null cosmological constant (Mattig 1958):

$$r = 2 \frac{c}{H_0} (1 - (1+z)^{-1/2}) \quad (1)$$

where c is the speed of light and $H_0 = 100 h \text{ km s}^{-1}/\text{Mpc}$ is the Hubble constant.

In the upper panel of Figure 2 we show the histogram of the distribution of XBACS (solid line) and BCS (dashed line) as a function of comoving distance. We have taken bins of comoving distance width $dr \simeq 35 h^{-1}\text{Mpc}$. The smooth curves are the fitting formulae proposed by FKP:

$$N(r) = 2^{(1+x/y)} N_{max} \left(\frac{r}{r_{max}} \right)^x \left[1 + \left(\frac{r}{r_{max}} \right)^y \right]^{-(1+x/y)} \quad (2)$$

with parameters quoted in Table 1 by a chi-square maximum like-hood method.

An often applied method to test for systematics gradients in the samples is to compute the observed comoving number density

$$n(r) = \frac{N(r)}{\Omega r^2 dr} \quad (3)$$

where $N(r)$ is the observed number of clusters in a bin at a distance r and Ω is the solid angle covered by the sample. Actually, the sky coverage is a function of the flux F , but this function is not available for these catalogues. Following Moscardini et al. (2000) we assume that the actual sky coverage is a constant, for XBACS is $\Omega = 4\pi(1 - \sin(b_{lim})) = 8.27$ and for BCS is $\Omega = 4.13$.

Since these are a flux limited samples we have normalized $n(r)$ to the expected comoving number density $n_0(r)$ obtained integrating the luminosity function,

$$n_0(r) = \int_{L_{min}}^{\infty} AL^{-\alpha} e^{L/L^*} dL, \quad (4)$$

where $L_{min} = 4\pi r^2(1+z)F_{lim}$. We have adopted the Schechter luminosity function parameters from Plionis & Kolokotronis (1998) and we quote them in Table 2.

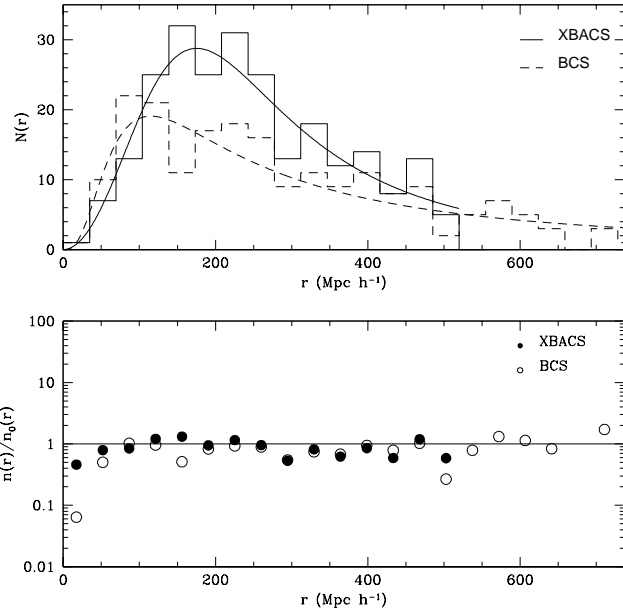


Figure 2. Upper panel: Histogram of the spatial distribution of XBACS (solid line) and BCS (dashed line). The smooth curves are the corresponding fitting formulae given by equation (2). Lower panel: Normalized comoving number density of XBACS (filled circles) and BCS (open circles) along the radial direction.

Table 2. Parameters of Schechter luminosity function. A units are $10^{-6} h^3 \text{Mpc}^{-3} (10^{44} h^{-2} \text{ergs}^{-1})^{\alpha-1}$. L^* units are $10^{44} h^{-2} \text{ergs}^{-1}$

sample	A	L^*	α
XBACS	1.955	1.048	1.21
BCS	1.246	2.275	1.85

In the lower panel of Figure 2, we plot the normalized comoving number density $n(r)/n_0(r)$ of XBACS (filled circles) and BCS (open circles). This plot shows the absence of spatial gradients in the samples. See Plionis & Kolokotronis (1998) for a detailed description of these effects.

3.3 The method

If the cluster sample has N_c clusters with vector positions \mathbf{x}_c we construct a random catalog with the same geometry and selection function of the sample with N_r points with vector positions \mathbf{x}_r . Then, we define a quantity with mean value zero as:

$$\delta(\mathbf{k}) = D(\mathbf{k}) - \alpha W(\mathbf{k}) \quad (5)$$

where

$$D(\mathbf{k}) = \sum_{c=1}^{N_c} \omega(x_c) e^{i\mathbf{k} \cdot \mathbf{x}_c} \quad (6)$$

is the Fourier transform of the cluster distribution, and

$$W(\mathbf{k}) = \sum_{r=1}^{N_r} \omega(x_r) e^{i\mathbf{k}\cdot\mathbf{x}_r} \quad (7)$$

is the Fourier transform of the window function of the survey. In Equation (5) $\alpha = S_c/S_r$ with

$$S_c = \sum_{c=1}^{N_c} \omega^2(x_c) \quad \text{and} \quad S_r = \sum_{r=1}^{N_r} \omega^2(x_r). \quad (8)$$

Assuming Gaussian density fluctuations, FKP derive a weight function

$$\omega(r) = \frac{1}{1 + n(r)P_w(k)} \quad (9)$$

that minimizes the power spectrum variance. To compute these weights the actual value of the power spectrum is needed. To solve this problem we propose different values for $P_w(k)$ as an initial guess. Having defined $\delta(\mathbf{k})$ by equation (5) the power spectrum estimator is obtained by:

$$P(\mathbf{k}) = (|\delta(\mathbf{k})|^2 - \alpha(1 + \alpha)S_r)/C \quad (10)$$

where C is a normalization constant defined by:

$$C = \alpha^2 \frac{1}{V} \sum_{i=1}^{N^3} (|W(\mathbf{k}_i)|^2 - S_r^{-1}) \quad (11)$$

and V is the volume where periodicity is assumed. We have adopted the above definition of $\alpha = S_c/S_r$ in order to recover the definition of $P(\mathbf{k})$ given by equation (2.4.5) of FKP. Finally, assuming isotropy we compute the power spectrum estimator averaging over spherical shells $k < |\mathbf{k}| < k + dk$ where there are N_k wavenumber vectors \mathbf{k}_i :

$$P(k) = \frac{1}{N_k} \sum_{i=1}^{N_k} P(\mathbf{k}_i). \quad (12)$$

We compute spectral densities at the multiples of the fundamental mode in order to avoid oversampling of the spectra that could produce spurious features. In order to compute the Fourier transform of the distribution of the cluster sample (equation (6)) and of the random catalogue (equation (7)) we use a Fast Fourier Transform (FFT) algorithm (Press et al., 1986). We compute these quantities embedding the distributions within a periodic larger cubic volume $V = r_{box}^3$ divided in N cells per side. To use FFT we assign the spatial distribution of points (clusters or random) into the grid by means of different weight assignment schemes.

3.4 Error estimations

We have estimated errors of the power spectrum using equation 2.4.6 of FKP:

$$\sigma^2(k) = \frac{2}{N_k^2} \sum_{i=1}^{N_k} \sum_{j=1}^{N_k} |P(k)Q(\mathbf{k}_i - \mathbf{k}_j) - S(\mathbf{k}_i - \mathbf{k}_j)|^2 \quad (13)$$

where

$$Q(\mathbf{k}) = \alpha \sum_{r=1}^{N_r} n(x_r) \omega^2(x_r) e^{i\mathbf{k}\cdot\mathbf{x}_r} / C \quad (14)$$

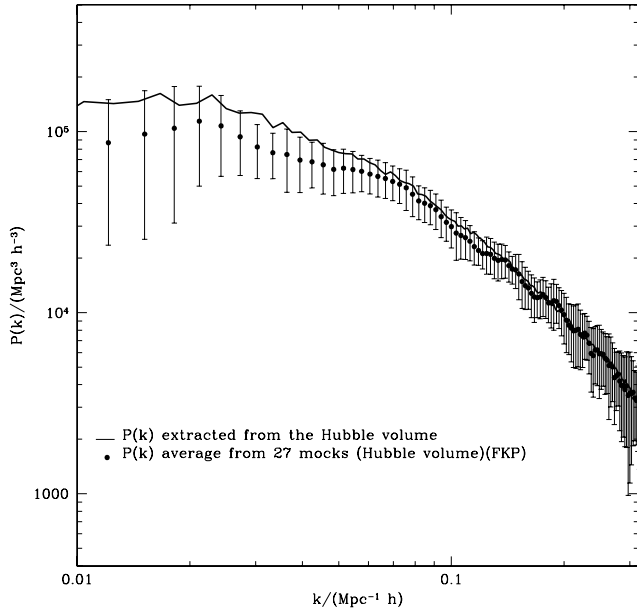


Figure 3. The solid line shows the power spectrum of haloes identified in the complete Hubble Volume Simulations and points are the average haloes power spectrum of 27 mocks catalogues extracted from the same simulation. The later was computed using the FKP formalism (eq.10). The error bars show the corresponding 1- σ standard deviation.

and

$$S(\mathbf{k}) = \alpha(1 + \alpha) \sum_{r=1}^{N_r} \omega^2(x_r) e^{i\mathbf{k}\cdot\mathbf{x}_r} / C. \quad (15)$$

In equation (13) \mathbf{k}_i and \mathbf{k}_j are assumed to belong to the same spherical shell $k < |\mathbf{k}| < k + dk$. Note that $S(\mathbf{k} = (0, 0, 0)) = \alpha(1 + \alpha)S_r$ is the second term of the definition of $P(\mathbf{k})$, equation (11).

3.5 N-body Simulations

In the previous section we have used equation 2.4.6 of FKP in order to estimate power spectrum errors. To test the error analysis of FKP we have used a second method based on the variance of $P(k)$ obtained from mock XBACS catalogue. We have constructed these mock catalogue from the Hubble volume simulations carried out by the Virgo Consortium (Jenkins et al. 1998). The simulation use 10^9 particles in a cubic volume of $3000 h^{-1} \text{ Mpc}$ per side resulting in a mass per particle of $2.25 \times 10^{12} h^{-1} M_\odot$. The initial condition were generated using the Lambda Cold Dark Matter (LCDM) model with the following parameters: dimensionless matter density $\Omega_m = 0.3$, dimensionless cosmological constant density $\Omega_\Lambda = 0.7$, $h = 0.7$ and relative mass fluctuation in a sphere of $8 h^{-1} \text{ Mpc}$ $\sigma_8 = 0.9$. This normalization is consistent both with the observed abundance at $z = 0$ of rich clusters and the fluctuations detected by the satellite COBE. From this simulation, we have used the haloes of particles kindly provided by Carlton Baugh identified using a standard "friends of friends" algorithm. The selected

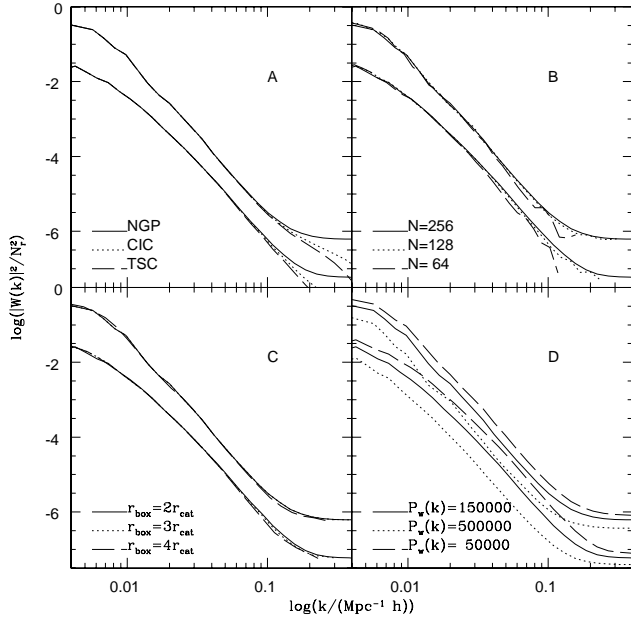


Figure 4. Dependence of XBACS (upper curves) and BCS (lower curves) window functions on different parameters (see labels). Panel A: weight assignment scheme. Panel B: number of grids N . Panel C: box side r_{box} . Panel D: guessed power spectrum $P_w(k)$. To make the plot clearer we have lowered the amplitude of BCS curves by one order of magnitude.

haloes have a mean separation of $d_c = 50h^{-1}$ Mpc in order to reproduce the same number of cluster of the catalogue. This choice is also consistent with the correlation length of $r_0 \simeq 21h^{-1}$ (Abadi, Lambas & Muriel, 1998) from the $r_0 - d_c$ relation obtained by Colberg et al. 2000. The volume of the simulation allows to extract 27 (3 per side) independent boxes with a side comparable to the XBACS cluster catalogue. In order to mimic some of the observational constraints, we have applied to each one of these boxes the same cuts in redshift and galactic latitude of the XBACS sample. Also, we convert center of mass positions of haloes from real to redshift space using the corresponding peculiar velocity of the halo (the conversion from comoving distance to redshift and viceversa was realized using equation 1). Finally, we convert total masses to X-ray luminosities using the empirical relation $M - L_X$ proposed by Reiprich & Böhringer 2000:

$$\frac{M}{h^{-1}M_\odot} = 4.7 \times 10^{14} \left(\frac{L_X}{10^{44} h^{-2} \text{erg/s}} \right)^{\frac{1}{1.243}} \quad (16)$$

We remove clusters with X-ray luminosity lesser than the luminosity limit which is given by (Peacock 2000)

$$L_{\text{lim}} = \frac{4\pi}{1+z} d_L^2(z) F_{\text{lim}} \quad (17)$$

where $F_{\text{lim}} = 5 \times 10^{-12} \text{erg s}^{-1} \text{cm}^{-2}$ in the energy range 0.1-2.4 keV and d_L is the luminosity distance

$$d_L = r(1+z) \quad (18)$$

with r given by equation (1).

Using the method described in section 3 we compute the power spectrum of each one of the 27 constructed mock

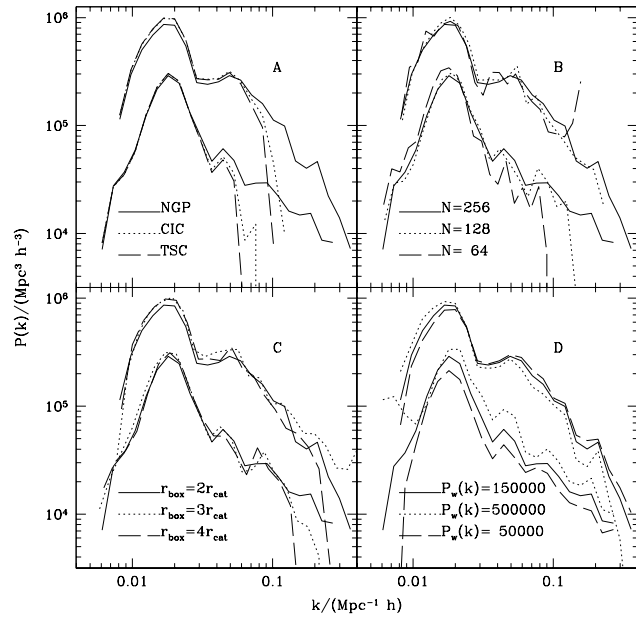


Figure 5. The estimated power spectrum of XBACS (upper curves) and BCS (lower curves). The different panels correspond to different mass assignment scheme, number of grids, weights and box size as indicated in Figure 3. The logarithmic amplitude of BCS power spectrum is shifted -0.5 to make the plot clearer.

catalogue and then we compute the mean power spectrum and the corresponding 1σ standard deviations. Using this model and parameters the haloes obtained have both a redshift space distribution and a power spectrum similar to XBACS.

In order to test the ability of the method to reproduce the correct power spectrum of clusters we compare the power spectrum of the haloes identified in the Hubble Volume Simulation with the average power spectrum of the 27 mocks catalogues using equation 10. We have computed the power spectrum of the Hubble Volume haloes using

$$P(k) = V_H \left(\frac{1}{N_h^2} \left| \sum_{i=1}^{N_h} e^{i\mathbf{k} \cdot \mathbf{x}_i} \right|^2 - \frac{1}{N_h} \right) \quad (19)$$

where V_H is the cubic volume of the Hubble simulation and N_h is the number of haloes identified in this volume.

In figure 3 the solid line is the power spectrum of Hubble Volume haloes and the points is the average haloes power spectrum of the 27 mocks catalogues. The error bars show the corresponding $1-\sigma$ standard deviations. For this comparison we have chosen haloes identified using $dc = 30 \text{Mpc}^{-1}$ in order to obtain a large number of haloes in each mock (~ 1000). This figure shows that the agreement between both estimates is very good for $k > 0.05 h \text{Mpc}^{-1}$ but for larger scales the power spectrum amplitude of the mocks catalogues is slightly lower. The error bars in the all range make the determinations undistinguishables showing that the method derived from FKP is a good estimator of power spectrum of a spatial distribution.

We also note that the method can take correctly into account the galactic extinction which can generate an over-

estimate of the amplitude in the power spectrum mainly on large scales (Vogele 1998).

4 DISCUSSION

First, we compute the window function of XBACS and BCS using equation (7). In Figure 4 we plot the window function module square $(|W(k)|/N_r)^2$ normalized to the number of points used to generate the random catalogue. For both samples, these random catalogue have $N_r = 10^6$ points distributed within the same geometrical limits of each sample and with the radial number density according to equation (3). In order to avoid superposition of XBACS and BCS curves in this Figure the amplitude of $(|W(k)|/N_r)^2$ for BCS is plotted with a factor 0.1. The window function can be very well approximated by a power law with index $n \simeq -4$ over the range $0.01h\text{Mpc}^{-1} < k < 0.1h\text{Mpc}^{-1}$ for both samples. This steep negative slope guarantees the validity of equation (10) (see Tadros & Esfathiou 1996). In the first three panels we test different parameters involved in the application of the FFT technique: panel A, weight assignment scheme; panel B, number of grids per side N and panel C, the box side r_{box} . In the last panel (D), we show the results of changing the guess value for the power spectrum $P_w(k)$ in the weight function using equation (9). In panel A it can be appreciated the effects of three different weight assignment schemes: nearest grid point (NGP, solid line), cloud in cell (CIC, dotted line) and triangular shaped cloud (TSC, dashed line). These weight assignments produce similar window functions although the discreteness smearing effects in the high-order scheme are nontrivial (Jing & Valdarnini, 1993). In panel B we show $(|W(k)|/N_r)^2$ using different values of $N = 256$ (solid line), 128 (dotted line) and 64 (dashed line). As it can be seen, at large wave-numbers the increase of N produces a smoother window function. In panel C we display the results for different box sides $r_{box} = 2, 3$ or 4 r_{cat} where r_{cat} is the minimum box side that contains the total cluster catalogue ($r_{cat} = 1037.1h^{-1}\text{Mpc}$ for XBACS and $r_{cat} = 1384.9h^{-1}\text{Mpc}$ for BCS). As it can be seen in this panel, they are indistinguishable. In panel D we show the dependence of the window function on the guess value, $P_w(k) = 150000$ (solid line), 500000 (dotted line) and 50000 $h^{-3}\text{Mpc}^3$ (dashed line). The window function amplitude is a monotonally decreasing function of $P_w(k)$. This dependence is relevant for the power spectrum determination of BCS and almost negligible for XBACS (see panel D in Figure 5). We recall that the FKP method is valid for wave-numbers where the window function is a factor 2 lower than its value at the origin (Tegmark et al. 1998). In our case this corresponds approximately to $k > 0.01h\text{Mpc}^{-1}$.

In Figure 5 we show the estimated redshift space power spectrum where the 4 panels correspond to those of Figure 4. To make this plot clearer the logarithmic amplitude of BCS power spectrum was shifted -0.5. Panel A shows a strong suppression of power at high frequencies which is more significant than in the window function plotted in Figure 4A. At low wave-number the agreement between the three schemes (NGP, CIC and TSC) is remarkably good. The increase of the spatial resolution using a larger number of cells per side produces a smoother power spectrum which can be appreciated in panel B. We have changed the guess

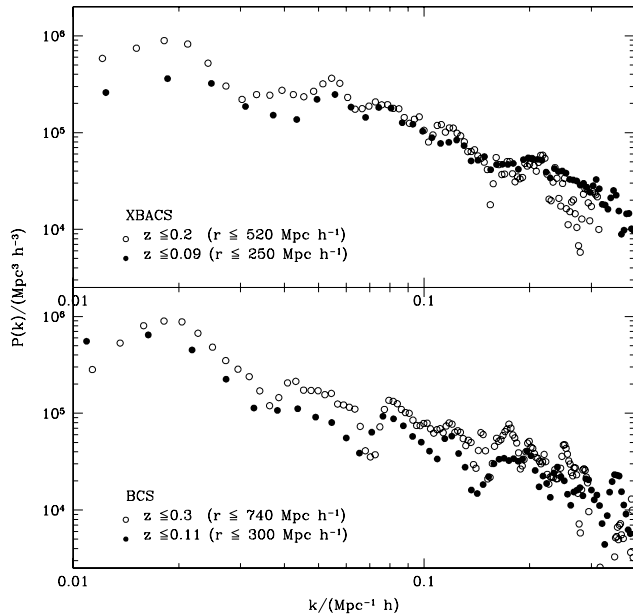


Figure 6. The upper panel shows the power spectrum for the complete XBACS (open circles) and the power spectrum for the XBACS clusters with $z \leq 0.09$ (filled circles). The lower panel shows the power spectrum for the complete BCS (open circles) and the power spectrum for the BCS cluster with $z \leq 0.11$ (filled circles).

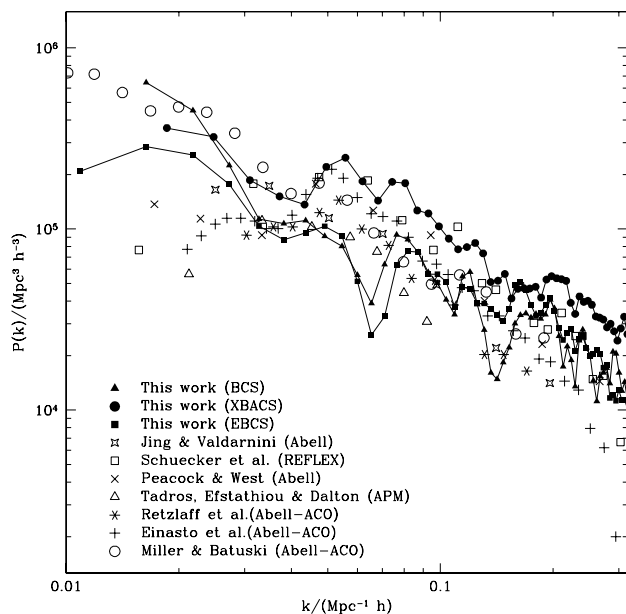


Figure 7. Comparison of the redshift space power spectrum of X-ray clusters with other samples obtained by different authors as indicated in the labels.

value $P_w(k)$ in the range $50000 h^{-3} \text{Mpc}^3 - 500000 h^{-3} \text{Mpc}^3$ finding that the results are not strongly dependent on the particular choice of this value. We also find that the results do not change substantially for box sides $r_{box}=2, 3$ and $4 r_{cat}$. Accordingly, we have used the NGP weighting assignment with parameters $N = 256$, $r_{box} = 2r_{cat}$ and $P_w(k) = 150000 h^{-3} \text{Mpc}^3$. We have also tested the dependence of the window function and power spectrum results on the method used (equation (3) or equation (4)) to estimate the cluster number density $n(r)$ finding no significant differences in the results. In what follows we adopt the FKP fit (equation (3)).

In order to test the presence of systematics effects that could artificially increase the amplitude of the power spectrum at large scales ($k \leq 0.03 h \text{Mpc}^{-1}$) (but see Miller & Batuski 2000), we have restricted our samples to smaller subsamples. Following Plionis & Kolokotronis (1998) we have generated two subsamples introducing a cut at $z \leq 0.09$ for XBACS and $z \leq 0.11$ BCS. In Figure 6 we show the corresponding power spectrum of each subsample compared with the power spectrum of the complete sample (Upper panel for XBACS and lower panel for BCS). From this comparison we observe a decreasing amplitude of the power spectrum in both subsamples mainly in large scales. Since we know that in large scales the fluctuation signal have a very low level, even small systematic errors inherent to the survey construction can cause and overestimate of the power spectrum in that scales. Consequently, we adopt this subsamples like a more accurate estimator of the power spectrum for the XBACS and BCS.

In Figure 7 we plot the redshift space power spectrum of XBACS (filled circles) and BCS (filled triangles). We have also computed the power spectrum of the recently released EBCS (filled squares) for $z \leq 0.11$. We compare our estimates with results obtained by other authors for different (optical and X-ray) cluster samples. The power spectrum obtained for XBACS has a higher amplitude than any other sample mainly in the range $k \geq 0.05 h \text{Mpc}^{-1}$.

Since in Figure 7 we find different amplitude between XBACS and BCS we have tested if this discrepancy could be explained by the fact that both samples have different limiting flux. Moscardini et al. (2000) show that for a given sample varying the limiting flux change the amplitude of the power spectrum but not the shape. In order to investigate this point, we have taken a subsample of the BCS catalogue with the same redshift and flux limit that XBACS and computed the power spectrum of this subsample. The obtained power spectrum for this subsample is very similar to the power spectrum for the complete BCS. From the comparison we conclude that the small variation in the limiting flux do not explain the different amplitude observed in Figure 7 between XBACS and BCS. Moreover, Ebeling et al. (1998) suggest that different fluxes could be assigned to a given cluster due to for example to different correction factors. This kind of differences can cause clusters to have the flux limit of $5.0 \times 10^{-12} \text{erg cm}^{-2}/\text{s}$ when the BCS fluxes are used, while they remain just below the flux limit in the XBACS. Another possibility to explain the different amplitudes is that XBACS could be richer and probably more massive than BCS that includes Abell, Zwicky and X-ray selected clusters with a poor optical counter-part. The power spectrum of XBACS is in good agreement with the power

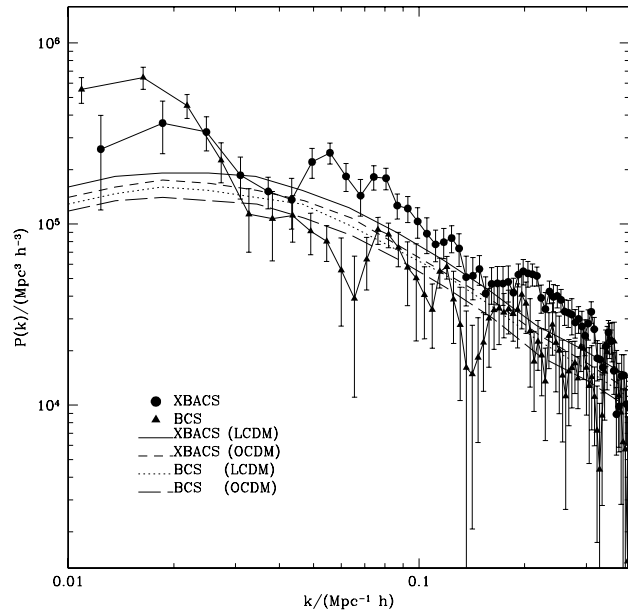


Figure 8. Comparison of the redshift space power spectrum of XBACS (filled circles) and BCS (filled triangles) with theoretical models computed by Moscardini et al. (2000) as indicated in the labels. The error bars are computed using equation (13) for $k < 0.1 h \text{Mpc}^{-1}$ and bootstrapping technique for $k > 0.1 h \text{Mpc}^{-1}$.

spectrum of the REFLEX (Schuecker et al. 2001) cluster survey for $k \gtrsim 0.03$. We do not find strong evidence of a peak at wave-numbers $\sim 0.05 h \text{Mpc}^{-1}$, consistent with the results found by Miller & Batuski (2000). We find a flattening of the power spectrum at these wave-numbers, smoother for XBACS than for BCS. The power spectrum of EBCS has a shape comparable to the original BCS except in large scales. In that scales, the BCS power spectrum have a higher amplitude.

In Figure 8 we present the power spectrum error bars of XBACS and BCS computed using the N-body simulations (section 3.3). This errors have comparable size to errors obtained using equation 13 even they are internal errors that do not take into account any source of systematic errors or cosmic variance. We also plot the power spectrum predictions given by Moscardini et al. (2000) for the two samples in two different cosmological models: Open Cold Dark Matter (OCDM) and Lambda Cold Dark Matter (LCDM). Both models have a dimensionless matter density parameter $\Omega_m = 0.3$ but a dimensionless cosmological constant $\Omega_\Lambda = 0$ for OCDM and $\Omega_\Lambda = 0.7$ for LCDM. The normalization of the models is in agreement with observed cluster abundances (root mean square mass fluctuation on a sphere of radius $8 h^{-1} \text{Mpc}$, $\sigma_8 = 0.87$ for OCDM and $\sigma_8 = 0.93$ for LCDM). Moscardini et al. (2000) also present the SCDM, τ CDM and TCDM models, but due to their significantly lower amplitudes we do not included them in the comparison. From this plot it is possible to note that the observational estimates for XBACS are consistent in shape with the prediction of Moscardini et al. (2000) model for both OCDM and LCDM but with an amplitude ~ 1.4 higher than the models. That is probably an indication that these

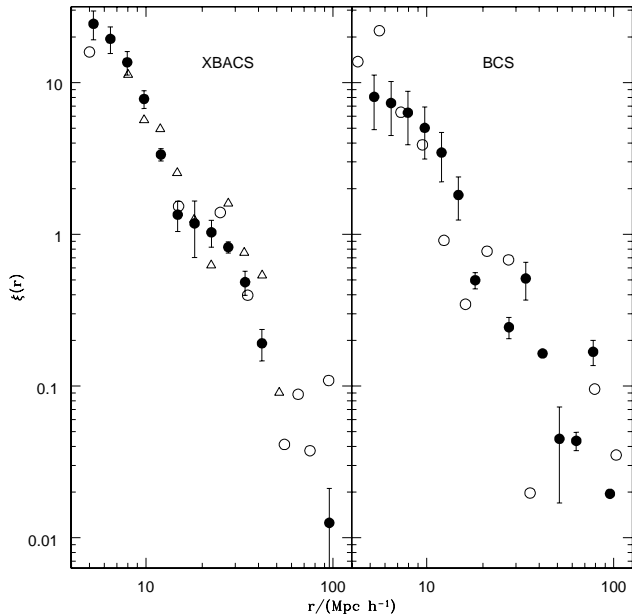


Figure 9. In the left panel we plot the two point correlation function of XBACS (filled circles) applying equation (17) to the previously determined power spectrum. We also show the results of Abadi, Lambas & Muriel (1998) (open circles) and Borgiani, Plionis & Kolokotronis (1999) (open triangles). In the right panel we plot the two point correlation function of BCS using equation (16) (open circles) and (17) (filled circles).

clusters that have a previous optical identification are very massive. For BCS the agreement with theoretical predictions is better in the range $k \geq 0.03hMpc^{-1}$. As pointed out in Section 3 we can not take into account the ROSAT exposure time across the survey, i.e. we not use the sky coverage of the satellite because this is not available for any of this catalogues. We know that variation can affect the measured power spectrum especially on large scales. Consequently, this could be the reason of a very high amplitude of BCS power spectrum at large scales ($k \leq 0.03hMpc^{-1}$). The reality of the ‘big bump’ at $k = 0.015hMpc^{-1}$ could be analyzed in more detail when the survey selection functions of the samples are taken into account properly if there were publically available. Moreover, the inhomogenous selection of clusters in the (E)BCS samples as well as the incompleteness of XBACS and eBCS of 80 percent and below 75 percent, respectively, could introduce some artificial fluctuations. This might give also an explanation of the high fluctuation power detected on scales larger $400h^{-1}Mpc$ compared to LCDM or OCDM models.

In order to test our results we derive an estimate of the two point correlation function from the power spectrum obtained previously. There are different ways to estimate the two point correlation function of a sample. One possibility is to derive it directly form the spatial distribution (Peacock 1999):

$$\xi(r) = \langle DD \rangle / \langle DR \rangle - 1 \quad (20)$$

where $\langle DD \rangle$ refers to the number of pair data-data separated by distance r and $\langle DR \rangle$ refers to the same quan-

tity for data-random pairs. This approach is the one applied by Abadi, Lambas & Muriel (1998) and Borgani, Plionis & Kolokotronis (1999) to XBACS. Other possibility is to estimate $\xi(r)$ using the relation between the power spectrum and the correlation function as Fourier transform pairs:

$$\xi(r) = \frac{1}{2\pi^2} \int_0^\infty P(k) k^2 \frac{\sin kr}{kr} dk. \quad (21)$$

In Figure 9 we have compared these two methods to estimate $\xi(r)$. For XBACS (left panel) we show the determination of $\xi(r)$ using equation (16) given by Abadi, Lambas & Muriel (1998) (open circles) and Borgani, Plionis & Kolokotronis (1999) (open triangles). We also plot our determination of $\xi(r)$ using the estimation of the power spectrum shown in Figure 6 though equation (21) (filled circles). This plot shows that there is a very good agreement between these three determinations. For BCS (right panel) we have computed $\xi(r)$ using both methods: equation (20) (open circles) and equation (21) (filled circles). We find a reasonably agreement between the methods. Error bars of $\xi(r)$ are obtained from the power estimation uncertainties propagated through equation (21).

5 CONCLUSIONS

In this paper we apply the method proposed by FKP to compute the redshift space power spectrum of two flux limited X-ray cluster samples: the XBACS and the BCS. At large wave-numbers $0.05hMpc^{-1} \lesssim k \lesssim 0.3hMpc^{-1}$ we find a power law behavior $P(k) \propto k^n$ with $n \simeq -1.2$ for XBACS and $n \simeq -1.0$ for BCS. The power spectrum of XBACS is consistent with that of the REFLEX cluster sample. It should be remarked that the power spectrum amplitude of XBACS and REFLEX are significantly higher than the one derived for optical samples, which are quite consistent with our BCS determination. We do not detect the presence of any strong peak near $0.05hMpc^{-1}$ supporting the idea that the presence of such a feature could be associated with biases in the samples (Miller & Batuski 2000). The OCDM and LCDM models of Moscardini et al. (2000) produce a good fit for BCS over a long range of wave-numbers, but underestimates the amplitude for XBACS. The shape of any of these models is also inconsistent with the shape obtained for XBACS. The correlation function of XBACS and BCS derived from the power spectrum agree with direct determinations (Abadi, Lambas & Muriel 1998 and Plionis & Kolokotronis 1998, this work).

ACKNOWLEDGMENTS

We thanks to the referee Peter Schuecker for very useful suggestions that improved the original version of the paper. We also thanks to Carlton Baugh for making available the haloes of the Virgo simulation and helpful discussions. We thanks to Astronomical Data Center (ADC) for different catalogue made available to test our power spectrum estimator. This work has been partially supported by the Consejo de Investigaciones Científicas y Técnicas de la República Argentina (CONICET), the Consejo de Investigaciones Científicas y

Tecnológicas de la Provincia de Córdoba (CONICOR), Secretaría de Ciencia y Tecnología de Universidad Nacional de Córdoba (SeCyT) and Fundación Antorchas, Argentina.

Scale Structure”, Ringberg Workshop on Large-Scale Structure, Kluwer, Amsterdam, astro-ph/9805160.

REFERENCES

- Abadi M.G., Lambas D.G., Muriel H., 1998, ApJ, 507, 526
Abell G.O., 1958, ApJS, 3, 211
Abell G.O., Corwin H.C. & Olowin R.P., 1989, ApJS, 70, 1
Bohringer H., Guzzo L., Collins C.A., Neumann D.M., Schindler S., Schuecker P., Cruddace R., Degrandi S., Chincarini G., Edge A.C., Macgillivray H.T., Shaver P., Vettolani G., Voger W., 1998, The messenger, 94, 21 (astro-ph/9809382)
Borgiani S., Plionis M., Kolokotronis V., 1999, MNRAS, 305, 866
Colberg J. M., White, S. D. M., Yoshida, N., MacFarland T. J., Jenkins, A., Frenk, C. S., Pearce, F. R., Evrard, A. E., Couchman, H. M. P., Efstathiou, G., Peacock, J. A., Thomas, P. A. (The Virgo Consortium), 2000, MNRAS, 319, 209
Dalton G.B., Maddox S.J., Sutherland W.J., Efstathiou G., 1997, MNRAS, 289, 263.
Ebeling H., Voges W., Bohringer H., Edge A.C., Huchra J.P. & Briel U.G., 1996, MNRAS, 281, 799
Ebeling H., Edge A.C., Bohringer H., Allen S.W., Crawford C.S., Fabian A.C., Voges W. & Huchra J.P., 1998, MNRAS, 301, 881
Ebeling H., Edge A.C., Allen S.W., Crawford C.S., Fabian A.C. & Huchra J.P., 2000, astro-ph/0003191
Einasto J., Einasto M., Gottlober S., Muller V., Saar V., Starobinsky A.A., Tago E., Tucker D., Andernach H., Frish P., 1997, Nature, 385, 139
Einasto J., Gramann M., Saar E., Tago E., 1993, MNRAS, 260, 705
Feldman H.A., Kaiser N., Peacock J.A., 1994, ApJ, 426, 23 (FKP)
Jenkins A., Frenk C.S., Pearce F.R., Thomas P.A., Colberg J.M., White S.D.M., Couchman H.M.P., Peacock J.A., Efstathiou G.P., Nelson A.H. (The Virgo Consortium), 1998, ApJ, 499, 20
Hoyle F., Baugh C.M., Shanks T., Ratcliffe A., 1999, MNRAS, 309, 659
Jing Y.P., Valdarnini R., 1993, ApJ, 406, 6
Mattig W., 1958, Astron. Nach., 284, 109
Miller C. & Batuski D.J., 2000, ApJ, submitted (astro-ph/0002295)
Moscardini L., Matarrese S., Lucchin F., Rosart P., 2000, MNRAS, accepted (astro-ph/9909273)
Peacock J.A., West M.J., 1992, 259, 494
Peacock J.A., Cosmological Physics, Cambridge University Press, 1999
Plionis M., Kolokotronis V., 1998, 500, 1
Press W.H., Flannery B.P., Teukolsky S.S. & Vetterling W.T., Numerical Recipes, Cambridge University Press, 1986
Reiprich T.H. & Böhringer H., 2000, in preparation
Retzlaff J., Borgani S., Gottlober S., Klypin A., Muller V., 1998, NewA, 3, 631
Schuecker, P., Böhringer, H., Guzzo, L., Collins, C.A., Neumann, D.M., Schindler, S., Voges, W., De Grandi, S., Chincarini, G., Cruddace, R., Müller, V., Reiprich, T.H., Retzlaff, J., Shaver, P., 2001, A&A, 368, 86.
Sutherland W., Tadros H., Efstathiou G., Frenk C.S., Keeble O., Maddox S., McMahan R.G., Oliver S., Rowan-Robinson M., Saunders W. White S.D.M., 1999, MNRAS, 308, 289
Tadros H., Efstathiou G., Dalton G., 1998, MNRAS, 296, 995
Tegmark M., 1995, ApJ, 455, 429
Tegmark M., Hamilton A.J.S., Strauss M.A., Vogeley M., Szalay A., 1998, ApJ, 499, 555.
Vogeley M., 1998, "Toward High-Precision Measures of Large-